Synthesis of mesoporous silica nanoparticles and nanorods: Application to doxorubicin delivery

Saher Rahmani, Jean-Olivier Durand, Clarence Charnay, Laure Lichon, Mokhtar Férid, Marcel Garcia, Magali Gary-Bobo

Synthesis of mesoporous silica nanoparticles and nanorods: application to doxorubicin delivery.

Saher Rahmani,[a-b] Jean-Olivier Durand,[a] Clarence Charnay,[a*] Laure Lichon,[c] Mokhtar Férid,[b] Marcel Garcia,[c] and Magali Gary-Bobo[c]

a. *Institut Charles Gerhardt Montpellier, UMR 5253, CC 1701 Equipe Ingénierie Moléculaire et Nano-objets, Place Eugène Bataillon, 34095 Montpellier Cedex 05,France. E-mail: clarence.charnay@umontpellier.fr.*

b. *Laboratoire de Physico-Chimie des Matériaux Minéraux et leurs Applications, Centre National de Recherches en Sciences des Matériaux, B.P. 95, Hammam-Lif, 2050, Tunisia.*

c. *Institut de Biomolécules Max Mousseron, UMR 5247, Avenue Charles Flahault, 34093 Montpellier Cedex 05, France, E-mail: magali.gary-bobo@inserm.fr.*

Abstract

The synthesis and application of mesoporous silica nanoparticles (MSN) and mesoporous silica nanorods (MSNR) for drug delivery were described. MSN or MSNR were obtained by adjusting the amount of added cosolvent to the sol-gel solution. Therefore, the addition of ethanol (EtOH) has contributed to the control of the particle shape and to the structure of the mesoporosity. MSN and MSNR particles were then loaded with doxorubicin and incubated with MCF-7 breast cancer cells. MSN and MSNR particles were efficient in killing cancer cells but their behavior in drug delivery was altered on account of the difference in their morphology. MSN showed a burst release of doxorubicin in cells whereas MSNR showed a sustained delivery of the anti-cancer drug.

Introduction

Mesoporous silica nanoparticles referred to as MSN have attracted considerable attention for biological applications, particularly those in the field of drug delivery that was extensively reviewed the last decade.[1-30] Indeed MSN exhibited key features such as tunable porosity from MCM-41 and MCM-48 type systems to radial porosity, very high specific surface area, tunable particle size, high drug loading capacities and biocompatibility which make them highly suitable for drug carriers. Since the pioneering work of Chung-Yuan Mou's[31] and Victor Lin's group, [32-34] mesoporous silica nanorods (MSNR) of MCM-41 and SBA-15[35] types were synthesized and used as nanocarriers, [36-38] for photodynamic therapy combined with drug delivery, [39] or to encapsulate MRI contrast agents. [40] The control of the shape of MSNR was achieved through a fine control of the pH[31] or using a structure co-directing agent such as perfluoro-octanoic acid[37] most often associated with a cationic surfactant such as cetyltrimethylammonium bromide. However co-surfactant systems were not required when co-condensation routes were applied since the organosilane precursors strongly influences the final particle morphology.[39,41] Furthermore, it was also highlighted that the size and shape of MSN affected their uptake in cancer cells, [36,37,42] with rods being more efficient than spheres[37]. However, this effect was also related to the cell line[32] and the nature of the nanocarrier (we recently reported that periodic mesoporous organosilica nanospheres were more endocytosed than nanorods).[43] Moreover, MSNR were shown to overcome multidrug resistance in cancer cells.[36] In the present paper, it was first investigated another route to control the MSN morphology. In this way, the influence of ethanol (EtOH) as co-solvent was studied for the synthesis of MSN type nanoparticles, and it was demonstrated that the very small amount of EtOH determined the shape of the nanomaterial. Besides, it was previously established that high molar ratio of $EtOH/H_2O$ were successful to control the pore structure and also the pore diameter.[44-46] Spheroidal or rod-like MSN were then loaded with doxorubicin (DOX) and incubated with MCF-7 cancer cells. A kinetic study revealed notable differences in the behavior of MSN particles with different shape.

Material and methods

Chemicals

Trimethyloctadecylammonium bromide (C_{18}TAB, 98%), tetraethyl orthosilicate (TEOS, 99.8%), ethanol (EtOH, 99.8%), ammonium nitrate (NH_4NO_3, 98%) and Doxorubicin hydrochloride (DOX) were purchased from Sigma-Aldrich. Standard solutions of sodium hydroxide (2M NaOH) were purchased from CARLO ERBA. All the solvents were used without further purification.

Synthesis of mesoporous silica nanoparticles

In a typical synthesis, 100 mg of the surfactant C_{18}TAB used as the porosity template, 50 mL of ultrapure water (18 MΩ cm) and EtOH (1 mL for MSN, 5 mL for MSNR) were stirred at 323 K for 20 minutes at 750 rpm in a 100 mL round bottomed flask. Then, a silica precursor TEOS (575 µL) and sodium hydroxide (350 µL, 2M) were added. The condensation process was conducted for 2 hours at 323 K. Then, the solution was cooled to room temperature while stirring to prevent the aggregation of the NPs, and collected by centrifugation for 15 minutes at 5200 g. The sample was then extracted twice with an alcoholic solution of NH_4NO_3 (6 $g.L^{-1}$) in order to remove the surfactant from the porosity and washed three times with ethanol, water, and ethanol. Each extraction involved a sonication step of 30 minutes at 323 K. Finally, the as-prepared material was dried under vacuum for few hours.

Materials characterizations

TEM pictures were recorded with a JEOL 1200 EX microscope. For this purpose, the particles were dispersed in ethanol and then dropped onto copper grids coated with porous carbon films.

The specific surface area and the pore structure parameters were determined from the measurements of nitrogen adsorption-desorption at 77 K on a Micromeritics ASAP 2020 V3.00 H unit. The pore volume and pore diameter were calculated by the Barrett-Joyner-Halenda (BJH) method. Prior to the sorption experiment, the sample (about 50 mg) was evacuated under vacuum at 393 K for 12 h. Small-angle powder X-ray diffraction (*sa*-XRD) measurements were performed with a PANalytical X'Pert MPD (Philips 1710) diffractometer. The XRD patterns were collected using a Cu Kα (λ = 0.15418 nm) radiation; the 2θ diffraction angles in the range from 1° to 7° was recorded at a rate of 0.5 deg min^{-1}. Dynamic light scattering analyses were performed in ethanol using a Cordouan Technologies DL 135 Particle size analyzer instrument. The size distributions were displayed in intensity mode. UV-Vis absorption spectra were recorded on a Hewlett-Packard 8453 Spectrophotometer.

Drug loading in MSN and MSNR

MSNs (10.3 mg) were first dispersed in a mixture of water (1 mL) and doxorubicin (3.5 mg) within an eppendorf tube. The dispersion was sonicated for 5 minutes in a bath at 318 K, and hydrochloric acid (0.02M) was added to reach pH 5.5 in order to improve the DOX diffusion into the porosity. The dispersion was then stirred overnight at room temperature.

Afterwards, the solution was neutralized with sodium hydroxide to trap the DOX at the pore surface. Then, the NPs were collected by centrifugation for 12 minutes at 2600 g. The sample was washed several times with water and dried under vacuum. The loading capacities of DOX were determined from the UV-visible spectra of the supernatant fluid after each wash.

The loading capacity (wt %) was defined as [mass of loaded drug/ (mass of loaded drug + mass of MSNs)]*100.

Cell culture

Human breast cancer cells (MCF-7) were purchased from ATCC (American Type Culture Collection, Manassas, VA). Cells were cultured in Dulbecco's Modified Eagle's Medium (DMEM-F12) supplemented with 10% foetal bovine serum and 50 µg mL^{-1} gentamycin. These cells were allowed to grow in humidified atmosphere at 310 K under 5% CO_2.

Drug delivery experiments

MCF-7 cells were seeded into 96-well plates at 2000 cells per well in 200 µL culture medium and allowed to grow for 24 h. Increasing concentrations of MSNA or MSNR containing doxorubicin were added in culture medium of MCF-7 cells. Three days after treatment, a MTT cell viability assay was performed to compare the drug delivery potential of the various batches. Briefly, cells were incubated for 4 h with 0.5 mg mL^{-1} of MTT (3-(4, 5-dimethylthiazol-2-yl)-2,5-diphenyltetrazolium bromide; Promega) in media. The MTT/media solution was then removed and the precipitated crystals were dissolved in EtOH/DMSO (v/v). The solution absorbance was read at 540 nm in a microplate reader.

Results and discussion

The addition of EtOH as a co-solvent to the sol-gel system was found to significantly change the morphology of MSN nanoparticles from spheroidal MSN (MSNA) to rod shaped MSN (MSNR) as observed on TEM micrographs in Fig. 1. Spheroidal monodisperse MSN (MSNA) were achieved for an added amount of 20µL of EtOH per mL of H_2O. The nanoparticles size distributions were confirmed through DLS analysis (Fig S.1) with a MSNA diameter centered on 300 nm and a narrow particle size distribution of 200 to 400 nm (Fig S.1). On the other hand, the addition of 100µL of EtOH per mL of H_2O has changed the particles shape into nanorods (MSNR) characterized by a lengthwise alignment of the pores channels (Fig. 1) and a diameter lying in the range of 450-650 nm (Fig S.1). MSN with a spherical shape, referred to as MSNB, were then obtained with a further increase of EtOH to 1 mL per mL of H_2O. However, MSNB particles exhibit a polydisperse size distribution as revealed on TEM micrographs (Fig.1) and an average diameter of 650 nm (Fig. S.1).

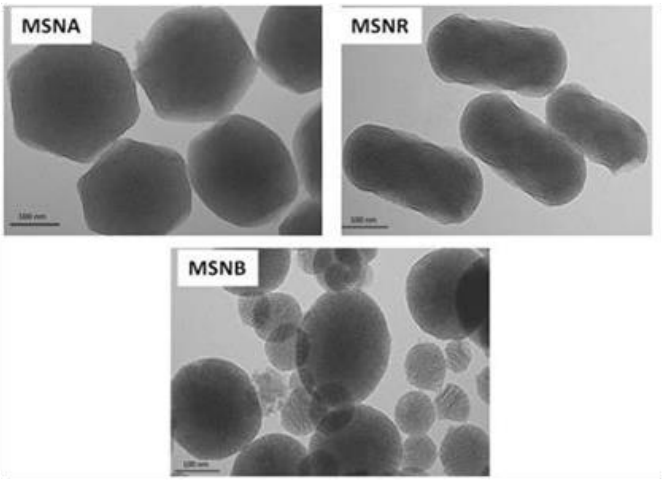

Fig. 1. TEM images of MSNA (EtOH: 20µL mL^{-1}), MSNR (EtOH: 100µL mL^{-1}) and MSNB (EtOH: 1mL mL^{-1})

Small-angle X-ray diffraction patterns (sa-XRD) are given in Fig 2. They exhibit a well-resolved diffraction line $2\theta < 3°$ assigned to the (100) reflection associated with a 2D hexagonal symmetry with a P6mm space group. Moreover MSNA and MSNR exhibit additional (110) and (200) reflections

characteristic of the MCM-41 hexagonal structure. However, the (110) and (200) reflections are unresolved for MSNB and difficult to be observed on account of the alteration the porosity arrangement. Indeed, it is observed on the TEM micrographs (Fig. 1) that the MSNB particles exhibit a radial porosity. Such a particular pore arrangement severely affects the pore hexagonal array and imposes some constraints that increase the disorder of the pore arrangement. These results emphasize that not only the shape of the MSNs is related to the added co-solvent but the organization of pores is changed also.

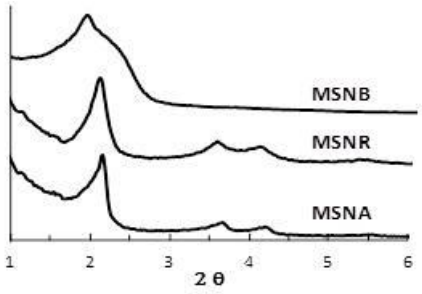

Fig. 2. Powder XRD patterns for MSNA, MSNR and MSNB samples

The nitrogen adsorption/desorption isotherms of the samples MSNA, MSNR and MSNB are shown in Fig.3. The three isotherms are of type IV according to the IUPAC classification, which is typical for mesoporous silica materials. All the samples exhibit a high specific surface area lying between 875 and 980 m^2 g^{-1}. The distribution of the pore (Fig.3) is calculated from the desorption branch of the isotherms using the BJH method. The BJH distributions are centred at 2.5 nm for MSNA and MSNB and at 2.9 nm for MSNR. Moreover, the mesopore filling takes place over a narrow range of relative pressures and the BJH distribution curves are scattered over relatively narrow areas in agreement with the uniform textural properties of the achieved materials.

The textural properties (high surface area and large pore volume) and the narrow particle size distribution, especially for MSNA and MSNR, are well suited for the proposed application of nanoencapsulation for drug delivery. Moreover MSNA and MSNR exhibit both a hexagonal organization of the porosity which enables a precise comparison of their properties of drug release, in contrast to MSNB sample exhibiting a high polydispersity of the particle size and a different organization of the porosity. It was indeed reported that particle morphology and pore structure affect the process of drug release.[47-49]

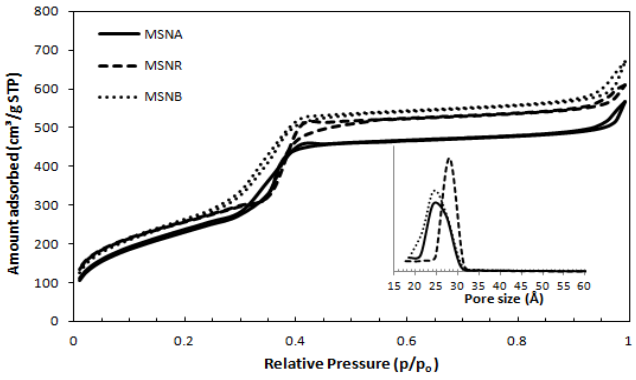

Fig. 3 Adsorption-desorption isotherms of N_2 at 77 K and BJH pore size distributions for MSNA, MSNR and MSNB samples

Effect of MSNs shape on drug delivery

Drug release was investigated to identify the effect of the particle morphology on the effectiveness of the drug loading and delivery (Fig 4). MSNA and MSNR were loaded with DOX at 20 wt % and 30 wt %, respectively. This demonstrated the better encapsulation efficiency of MSNR. Moreover, release experiments (Fig. 4) highlighted the stability at neutral pH of the encapsulated DOX for both MSNA and MSNR. The DOX release was triggered lowering the pH of the solution as already shown with hollow MSN.[50] This implies that the release of the encapsulated DOX into MSN can be effective following the internalisation of the loaded particles into the acidic compartments of the cell.

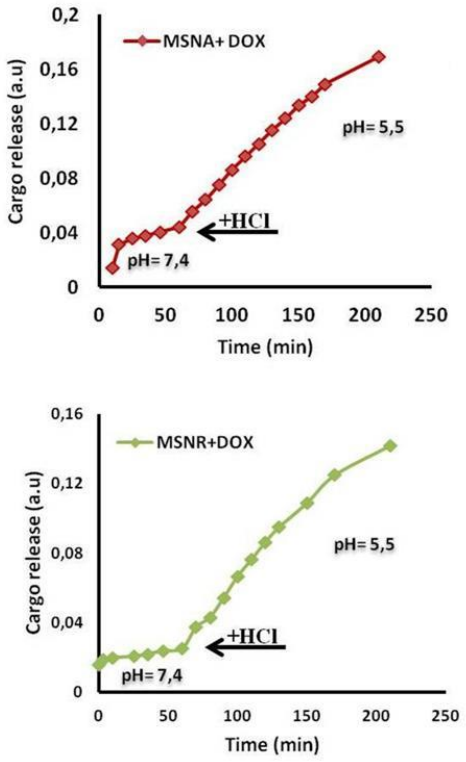

Fig. 4. Doxorubicin delivery triggered by pH lowering from 7.4 to 5.5 by the addition of HCl (2 M) as shown by the arrow. The release profiles are plotted from the UV-visible spectra of the released drug over time.

Assay of cytotoxicity in cancer cell line MCF-7

Since the release of DOX was pH sensitive, MSNA and MSNR were then incubated with MCF-7 cells for 72 h at various concentrations from 0 µg mL^{-1} to 200 µg mL^{-1} and the cytotoxicity of nanoparticles was examined using the MTT cell viability assay (Fig 5A and B). Results showed that empty MSNA were more toxic than MSNR. At low concentration below 5 µg mL^{-1}, MSNs exhibited no cytotoxicity. MSNA and MSNR were then loaded with doxorubicin and compared for their cytotoxic effects. From the results of MTT cell viability assay, we observed an important cytotoxicity at very low concentration of nanoparticles. Indeed, about 80% of MCF-7 cells were killed with a loaded MSN concentration of 5 µg mL^{-1} (Fig 5A and B).

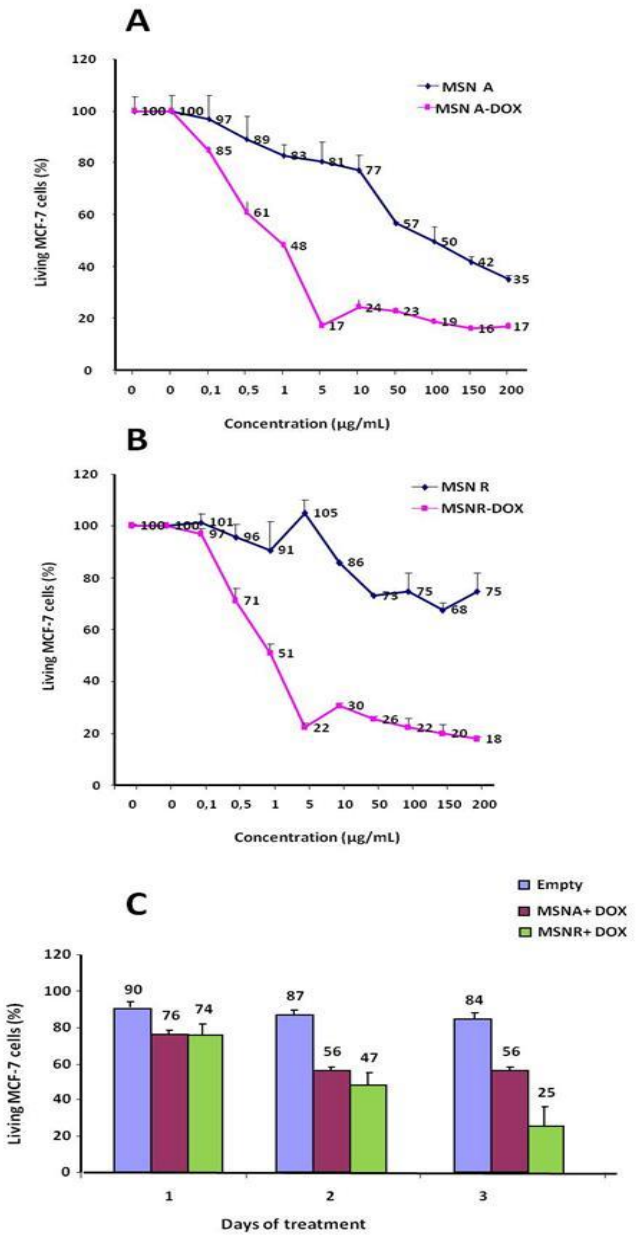

Fig. 5. DOX delivery in MCF-7 cancer cells via MSNA and MSNR. Cytotoxic study of a range (from 0.1 to 200 µg mL-1) of empty or loaded MSNA (A) or MSNR (B) incubated for 72 h with human breast cancer cells (MCF-7). Kinetic study of empty or full MSNA and MSNR (C) incubated for 1 to 3 days at a concentration of 1 µg mL^{-1}. Values are means ± standard deviation of 3 experiments.

In addition, kinetics studies were then performed at 1 µg mL^{-1} of MSNA and MSNR and the behaviour of both nanomaterials was different (Fig 5C). MSNR showed a sustained release of DOX over 72 h with a progressive cancer cell killing effect whereas MSNA showed a burst release of DOX after 24 h-48 h with no improvement of the cancer cell killing effect after 48 h. Finally, since MSNA and MSNR did not exhibit the same loading capacity of doxorubicin, they were incubated with MCF-7 cells for 72 h at equivalent concentrations of doxorubicin (Fig 6). The results showed that MSNA were very active at low concentration (12.35 ng mL^{-1} DOX equivalents) and increasing the concentration of MSNA did not improve the results. In contrast, loaded MSNR was less toxic at low concentration but increasing their concentration, the cancer cell killing effect was dramatically increased.

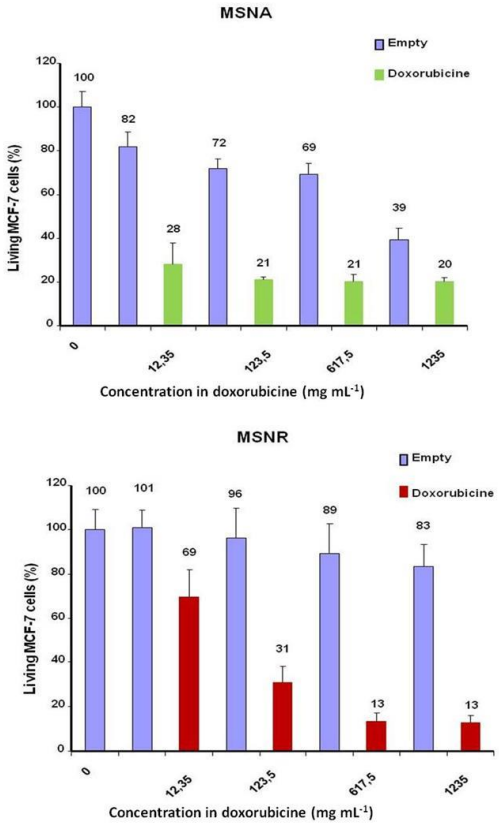

Fig. 6. Cytotoxicity of MSNA and MSNR in MCF-7 cells after 72 h of incubation at equivalent concentrations of doxorubicin (ng.mL^{-1}) and in comparison the effect of equivalent amount of unloaded MSNs (blue bars).

Conclusions

The control of the shape of mesoporous silica nanoparticles was successfully achieved by simply adjusting the amount of EtOH as a cosolvent during the sol-gel procedure. MSNR showed an increased of the DOX loading capacity compared to MSNA with a spheroidal morphology. The nanomaterials were used for DOX delivery in cancer cells and were both very efficient for cancer cell killing at very low concentrations. However the behaviour of the materials in cancer cells was different, MSNR showing a sustained release of DOX compared to MSNA. As a result, the formulation of drug carrier with MSN of different shape and morphology may enhance the control of the kinetic delivery with the possibility to associate burst and extended drug release.

Acknowledgements

Erasmus mundus Grant (Alyssa project) for Saher Rahmani is gratefully acknowledged.

References

1 N. Z. Knezevic and J.-O. Durand, *Nanoscale*, 2015, **7**, 2199-2209.
2 N. Z. Knezevic and J.-O. Durand, *ChemPlusChem*, 2015, **80**, 26-36.
3 Y. Zhang, J. Yan and S. Liu, *Biointerface Research in Applied Chemistry*, 2014, **4(3)**, 767-775.
4 K.-N. Yang, C.-Q. Zhang, W. Wang, P. C. Wang, J.-P. Zhou and X.-J. Liang, *Cancer Biology & Medicine*, 2014, **11**, 34-43.
5 P. Nadrah, O. Planinsek and M. Gaberscek, *J. Mater. Sci.*, 2014, **49**, 481-495.
6 Q. He and J. Shi, *Adv. Mater.*, 2014, **26**, 391-411.

7 P. N. Dave and L. V. Chopda, *Materials Sci. Forum*, 2014, **781**, 17-24.
8 C. Argyo, V. Weiss, C. Braeuchle and T. Bein, *Chem. Mater.*, 2014, **26**, 435-451.
9 S.-H. Wu, C.-Y. Mou and H.-P. Lin, *Chem. Soc. Rev.*, 2013, **42**, 3862-3875.
10 K. T. Mody, A. Popat, D. Mahony, A. S. Cavallaro, C. Yu and N. Mitter, *Nanoscale*, 2013, **5**, 5167-5179.
11 V. Mamaeva, C. Sahlgren and M. Linden, *Adv. Drug. Deliv. Rev.*, 2013, **65**, 689-702.
12 W. X. Mai and H. Meng, *Integr. Biol.,* 2013, **5**, 19-28.
13 N. Z. Knezevic, E. Ruiz-Hernandez, W. E. Hennink and M. Vallet-Regi, *RSC Adv.*, 2013, **3**, 9584-9593.
14 R. Duan, F. Xia and L. Jiang, *ACS Nano*, 2013, **7**, 8344-8349.
15 D. Douroumis, I. Onyesom, M. Maniruzzaman and J. Mitchell, *Crit Rev Biotechno*, 2013, **33**, 229-245.
16 Y. Chen, H. Chen and J. Shi, *Adv. Mater.*, 2013, **25**, 3144-3176.
17 N.-T. Chen, S.-H. Cheng, J. S. Souris, C.-T. Chen, C.-Y. Mou and L.-W. Lo, *J. Mater. Chem. B*, 2013, **1**, 3128-3135.
18 J. L. Vivero-Escoto, R. C. Huxford-Phillips and W. B. Lin, *Chem. Soc. Rev.*, 2012, **41**, 2673-2685.
19 F. Tang, L. Li and D. Chen, *Adv. Mater.*, 2012, **24**, 1504-1534.
20 Y.-S. Lin, K. R. Hurley and C. L. Haynes, *J. Phys. Chem. Letters*, 2012, **3**, 364-374.
21 T. Asefa and Z. Tao, *Chem. Res. Toxicol.*, 2012, **25**, 2265-2284.
22 Y.-W. Yang, *Medchemcomm*, 2011, **2**, 1033-1049.
23 A. Popat, S. B. Hartono, F. Stahr, J. Liu, S. Z. Qiao and G. Q. Lu, *Nanoscale*, 2011, **3**, 2801-2818.
24 Q. He and J. Shi, *J. Mater. Chem.*, 2011, **21**, 5845-5855.
25 J. L. Vivero-Escoto, I. I. Slowing, B. G. Trewyn and V. S. Y. Lin, *Small*, 2010, **6**, 1952-1967.
26 I. I. Slowing, J. L. Vivero-Escoto, B. G. Trewyn and V. S. Y. Lin, *J. Mater. Chem.*, 2010, **20**, 7924-7937.
27 K. K. Coti, M. E. Belowich, M. Liong, M. W. Ambrogio, Y. A. Lau, H. A. Khatib, J. I. Zink, N. M. Khashab and J. F. Stoddart, *Nanoscale*, 2009, **1**, 16-39.
28 B. G. Trewyn, I. I. Slowing, S. Giri, H.-T. Chen and V. S. Y. Lin, *Acc. Chem. Res.*, 2007, **40**, 846-853.
29 I. I. Slowing, B. G. Trewyn, S. Giri and V. S. Y. Lin, *Adv. Funct. Mater.*, 2007, **17**, 1225-1236.
30 S. Hermans, S. Sadasivan, C. M. G. Judkins, B. F. G. Johnson, S. Mann and D. Khushalani, *Adv. Mater.*, 2003, **15**, 1853-1857.
31 M.-C. Chao, H.-P. Lin and C.-Y. Mou, *Chem. Letters*, 2004, **33**, 672-673.
32 B. G. Trewyn, J. A. Nieweg, Y. Zhao and V. S. Y. Lin, *Chem. Engin. J.*, 2008, **137**, 23-29.
33 S. Giri, B. G. Trewyn, M. P. Stellmaker and V. S. Y. Lin, *Angew. Chem. Int. Ed. Engl.*, 2005, **44**, 5038-5044.
34 B. G. Trewyn, C. M. Whitman and V. S. Y. Lin, *Nano Lett.*, 2004, **4**, 2139-2143.
35 X. Ji, K. T. Lee, M. Monjauze and L. F. Nazar, *Chem. Commun.*, 2008, 4288-4290.
36 L. Li, X. Huang, T. Liu, H. Liu, N. Hao, D. Chen, Y. Zhang, L. Li and F. Tang, *J. Nanosci. Nanotechnol.*, 2012, **12**, 4458-4466.
37 H. Meng, S. Yang, Z. Li, T. Xia, J. Chen, Z. Ji, H. Zhang, X. Wang, S. Lin, C. Huang, Z. H. Zhou, J. I. Zink and A. E. Nel, *ACS Nano*, 2011, **5**, 4434-4447.
38 Z. Bahrami, A. Badiei and G. M. Ziarani, *J. Nanopart. Res.*, 2015, **17**, 1-12.
39 G. Yang, H. Gong, X. Qian, P. Tan, Z. Li, T. Liu, J. Liu, Y. Li and Z. Liu, *Nano Res.*, 2015, **8**, 751-764.
40 C. P. Tsai, Y. Hung, Y. H. Chou, D. M. Huang, J. K. Hsiao, C. Chang, Y. C. Chen and C. Y. Mou, *Small*, 2008, **4**, 186-191.
41 S. Huh, J. W. Wiench, B. G. Trewyn, S. Song, M. Pruski and V. S. Y. Lin, *Chem. Commun.*, 2003, 2364-2365.
42 J. Mo, L. He, B. Ma, and T. Chen, *ACS Appl. Mater. Interfaces*, 2016, **8**, 6811−6825
43 J. Croissant, X. Cattoen, M. W. C. Man, A. Gallud, L. Raehm, P. Trens, M. Maynadier and J.-O. Durand, *Adv. Mater.*, 2014, **26**, 6174-6178.
44 Y. He, H. X, S. Ma, P. Zhang, W. Huang, M. Kong, *Mater. Letters*, 2014, **131**,361–365
45 Y. He, , J. Li, , M. Long, S. Liang, H. Xu, *J. Non-Crystalline Sol.*, 2017, **457**, 9–12
46 W. Zhao, H. Zhang, S. Chang J. Gu, Y. Li, L. Lia and J. Shi, *RSC Adv.*, 2012, **2**, 5105–5107
47 P. Horcajada, A. Ramila, J. Perez-Pariente, M. Vallet-Regi, *Microporous & Mesoporous Mater.*, 2004, **68**, 105-109
48 X. Huang, N. P Young, and H. E Townley, Nanomater Nanotechnol, 2014, **4:2**,1-15
49 L. Wu, Z. Jiao, M. Wu, T. Song and H. Zhang, RSC Adv., 2016, **6**, 13303-13311
50 Y. Gao, Y. Chen, X. Ji, X. He, Q. Yin, Z. Zhang, J. Shi and Y. Li, *ACS Nano*, 2011, **5**, 9788-9798.